Research Square

Preprints are preliminary reports that have not undergone peer review.
They should not be considered conclusive, used to inform clinical practice,
or referenced by the media as validated information.

Single-Walled Carbon Nanotube and its Copper/Nitrogen dual-modified Derivatives as Biosensors for Liver Cancer Biomarkers: Insight from Computational Approach

Emmanuel A. Anyama

emmanuelayi05@gmail.com

University of Calabar

Chinyere A. Anyama

University of Calabar

Francisca Bassey

University of Cross River State

Ayi A. Ayi

University of Calabar

Research Article

Keywords: Carbon nanotube, Modification, liver cancer, biomarker, DFT

Posted Date: November 14th, 2026

DOI: https://doi.org/10.21203/rs.3.rs-11431717/v1

License: This work is licensed under a Creative Commons Attribution 4.0 International License.
Read Full License

Additional Declarations: No competing interests reported.

Single-Walled Carbon Nanotube and its Copper/Nitrogen dual-modified Derivatives as Biosensors for Liver Cancer Biomarkers: Insight from Computational Approach

[1] Emmanuel A. Anyama*, [2] Chinyere A. Anyama, [3] Francisca Bassey, and [4]Ayi A. Ayi

[1]Department of Pharmacology, University of Calabar, Calabar, Nigeria

[2]Department of Pure and Industrial Chemistry, University of Calabar, Calabar, Nigeria

[3]Department of Chemistry, University of Cross River State, Calabar, Nigeria

[4]Department of Pure and Industrial Chemistry, University of Calabar, Calabar, Nigeria

[*]**Corresponding author's email:** emmanuelayi05@gmail.com

Abstract

This study explores the modification of Single-Walled Carbon Nanotubes (SWCNTs) with nitrogen and copper for its application in the sensing of liver cancer biomarkers; hexanal (HXN), limonene (LMN), methanol (MTN), octenol (OTN) and pentanal (PTN). The study employed the M06-2X/D3/Def2svp level of theory for the optimization of the studied interactions, utilizing density functional theory (DFT) calculations. Natural bond orbital (NBO) analysis gave insight to the transfer of charges between the orbitals of the adsorbate and adsorbent, highlighting that adsorption took place. Adsorption energies ranged from −0.81 eV to −2.72 eV, indicating chemisorption across the studied complexes, with the more negative values suggesting stronger, more stable adsorbate–adsorbent interactions. Non-covalent interaction (NCI) analysis showed a mixture of interaction types within each complex: weak van der Waals forces were predominant in most systems, while steric repulsion dominated in MTN-@CuNCNT. Regions of strong, covalent-like interaction (denoted by blue in the NCI iso-surfaces) were also identified, indicating localized strong bonding contributing to the overall adsorption strength. The findings in this study suggest that modification of SWCNTs improved its performance, with promising results showing the potential of the modified surfaces to be used as sensors for liver cancer biomarkers.

Keywords: Carbon nanotube, Modification, liver cancer, biomarker, DFT

Introduction

The disease known as cancer is a health disorder characterized by the uncontrolled and or abnormal growth of cells in the human body **[1]**. Under normal conditions, the cells in the body grow, divide and die in a regulated process, but when cancer develops either by genetic or molecular changes disrupting those conditions, it causes the cells to keep multiplying when they should not **[1,2]**. These uncontrolled or abnormal cell growth may lead to the formation of a mass like tumor, although certain cancers like leukemia do not normally produce solid tumors **[3,4]**. These cancerous cells might then invade surrounding tissues and spread to other parts of the body through the blood or the lymphatic system, a process called metastasis **[5]**. There are different types of cancers which may include; cancer of the; breast, lung, prostate, stomach, liver and skin. Cancers may also be classified into groups such as carcinomas, sarcomas, leukemias, lymphomas and melanomas **[6]**. Cancer development is influenced by genetic, environmental and lifestyle factors, which are broken down into; tobacco use, excessive alcohol intake, exposure to certain chemicals or excess radiation, unhealthy diets, physical inactivity, increasing age or inherited genetic mutations **[7]**. Cancer symptoms may vary depending on the type and location of the disease and the warning signs may include; weight loss, unexplained pain, lumps or swellings, persistent cough, and changes in bowel and or bladder habits **[8]**. However, many cancers may not show their symptoms during their early stages, causing difficulty in detection. This set back has allowed scientist to come up with methods under biosensing for the early detection of cancer and other diseases that might also produce few to no symptoms in their early stages, as conventional diagnostic techniques are expensive and not easy to access.

Nanomaterials have emerged as promising candidates for early detection of diseases, with physical and chemical properties, large surface area, electrical and electronic properties, making them suitable for the conversion of biological interactions into measurable electrical signals **[9]**. Other properties of nanomaterials may include; good mechanical strength, thermal stability, catalytic activity, tunable surface chemistry and optical properties. One of these nanomaterials is the Single-Walled Carbon Nanotubes (SWCNTs) **[10]**. SWCNTs are cylindrical nanomaterials, which consist of a single sheet of sp^2-hybridized carbon atoms rolled into a continuous tube with diameters typically within the nanometer range **[11]**. The unique electronic and structural properties of SWCNTs depend strongly on their chirality, which describes how the graphene sheet is rolled to form the nanotube **[12]**. Based on their chirality, SWCNTs can exhibit either metallic or

semiconducting behavior making them applicable in electronic and sensing applications **[12,13]**. SWCNTs possess remarkable properties which include; high electrical conductivity, large surface to area volume, high mechanical strength, excellent thermal stability and strong chemical sensitivity **[14].** Their large surface area provides numerous sites for interaction with molecules, while their electronic properties allow for changes occurring on the nanotube surface to be translated into measurable electrical signals **[13,14]**. Despite these advantageous properties, SWCNTs suffer from a key limitation: insufficient selectivity toward specific biomolecules. To overcome this limitation, surface medication which mostly include doping and or functionalization have proven to be an excellent approach to making nanomaterials like SWCNTs sufficiently selective to specific biomolecules.

Aasi *et al.,* (2022) explored the potential of pristine and Platinum decorated SWCNTs as biosensors for liver biomarker, using octenol, decane and hexanal as the biomarkers. The study utilized density functional theory (DFT), employing the GGA-PBE functional with PBE-D2 dispersion correction. Their results illustrated that Platinum decoration significantly improved adsorption strength and charge transfer compared to pristine SWCNTs, indicating enhanced selectivity **[15]**. Rahimi *et al.,* (2025) explored a $B_3C_2N_3$ monolayer as a biosensor for liver cancer biomarkers using first principles DFT calculations. Their results indicated strong adsorption energies and noticeable electronic property changes upon molecule interaction, suggesting high sensitivity and selectivity **[16]**. Although not CNT based, the study on nitrogen functionalized carbon nano ribbons embedded with transitional metals (Fe and Co) used spin-polarized DFT to study adsorption of cancer related volatile organic compounds (VOCs) such as pentanal and methylglyoxal, provided a comparable theoretical framework for biomarker detection. Results showed that metal incorporation significantly enhanced adsorption strength and selectivity compared to undoped systems **[17]**. The observed changes in electronic and magnetic properties confirmed stability for sensing applications and also showing relevance as it showcased how modification with transition metals improves biomarker detection. However, none of these studies combined N- and Cu- co-doping on SWCNTs specifically for liver cancer VOC biomarkers.

This study presented a refined and targeted approach by utilizing copper and nitrogen atoms on SWCNTs for the selective detection of specific liver biomarkers; hexanal (HXN), limonene (LMN), methanol (MTN), octenol (OTN) and pentanal (PTN). The selection of the biomarkers was informed by their detection in the VOC profile associated with liver cancer, their potential

relationship with cancer related metabolic alterations and oxidative stress, and their potential ability to discriminate liver cancer patients from healthy individuals. Through DFT methods, this study offers deep insight into the biosensing abilities of the studied interactions. The improved sensitivity and selectivity after modification with copper and nitrogen, are highlighted.

2.0 Methodology

2.1 Computational details

M06-2X/D3/Def2svp level of theory was employed for the optimization of the studied compounds in this study, owing to its suitability for non-covalent interactions and dispersion-corrected weak-interaction systems **[18]**. Studied structures were sketched using GaussView 6.0.16 and visualized using Chemcraft where their bond lengths were extracted and recorded **[19,20]**. Frontier molecular orbital (FMO) analysis was carried out using Chemcraft, the energy gaps were calculated and the HOMO-LUMO iso-surface plotted. Gaussian 09W **[21]**, has an inbuilt natural bond orbital (NBO) algorithm which was used to carry out NBO analysis to determine the stability of the donor-acceptor interactions, usually from a bonding orbital (σ, π) or lone pair (LP) to an antibonding orbital (σ*, π*). Molecular electrostatic potential (MESP) was done using GaussView 6.0.16 to identify if electrophilic and nucleophilic attack sites are present on the studied structures. Multiwfn 3.8 software was utilized for non-covalent interactions (NCI) analysis for the identification of weak interactions and or strong covalent bonds **[22]**. All calculations were gas phase and carried out using the Gaussian 09W calculation setup, with the equations utilized as follows;

$$Eg = E_{LUMO} - E_{HOMO} \quad \textbf{(1)}$$

$$-\mu = {(E_{HOMO} + E_{LUMO})}/{2} \quad \textbf{(2)}$$

$$\eta = {(E_{HOMO} - E_{LUMO})}/{2} \quad \textbf{(3)}$$

$$\sigma = \left(\frac{1}{2\eta}\right) \quad \textbf{(4)}$$

$$\omega = \frac{(-\mu^2)}{2\eta} \quad \textbf{(5)}$$

$$E_{ads} = E_{complex} - (E_{surface} + E_{adsorbate}) \quad \textbf{(6)}$$

$$E_{sol} = (E_{water} + E_{gas}) \quad \textbf{(7)}$$

3.0 Structural Properties of Adsorbates

3.1 Bond Properties of the Studied Adsorbates

Geometry optimization was carried out on the adsorbates to enable structural stability and bond lengths observed were reported in **Table S1**. The geometry optimization results obtained for the studied adsorbates revealed slight variations in bond lengths when compared with standard bond length values, indicating the influence of electronic interactions, resonance effects, hybridization, and molecular environment on the structural arrangement of the molecules. The bond lengths observed generally aligned with standard values, and this confirmed structural stability of the optimized compounds. Looking at HXN, the C_8-H_{12} bond had a bond distance of 1.10 Å, which is slightly higher than the standard C-H bond length of approximately 1.09 Å. This slight increase could be attributed to weak electronic effects from neighboring atoms within the molecule **[23]**. The C_5-C_8 bond with bond distance of 1.53 Å was also close to the standard C-C single bond value of about 1.54 Å, the shortening suggested that the bond maintained normal single bond character. The C_1=O_2 bond length of 1.20 Å was exactly the standard carbonyl bond length of approximately 1.20 Å, indicating strong double bond character and effective electron sharing between the carbon and oxygen atoms **[23,24]**. In LMN, the C_6-H_{12} bond length of 1.10 Å corresponded with the normal C-H bond value, while the C_4-C_{15} bond length of 1.50 Å was slightly shorter than the standard C-C single bond length. This shortening may be caused by partial electron delocalization within the molecular framework and conjugative interactions around the carbon atoms **[24]**. The C_{19}=C_{20} bond length of 1.34 Å also corresponded with the standard C=C double bond value of approximately 1.34 Å, suggesting preserved double bond character in the optimized structure. MTN C_1-H_4 bond had a length of 1.11 Å, corresponding closely to the accepted standard value for C-H bonds, while the C_1-O_5 bond length of 1.40 Å was slightly shorter than the standard C-O single bond value of approximately 1.43 Å. This reduction could be resonance between interactions involving the oxygen atoms, that results in partial double bond character and stronger orbital overlap between the bonds. The H_6-O_5 bond length of 1.00 Å was close to the standard O-H bond length of 0.96 Å, this indicated the stability of the hydroxyl group within the molecule. In OTN, the C_7-H_9 bond length of 1.10 Å was close with the standard value, while the C_2-C_5 bond length of 1.51 Å remained within the normal range for carbon-carbon single bonds. The C_5-O_{24} bond length of 1.41 Å was slightly shorter than the standard value, also suggesting resonance stabilization involving the oxygen atom and electron donation from lone pair electrons. The H_{25}-

O_{24} bond length of 0.96 Å also indicated a stable hydroxyl bond. In addition, the C_1=C_2 bond length of 1.33 Å was slightly shorter than the standard C=C bond value, which may be due to increased electron density around the double bond region and greater π-electron interactions within the molecular structure **[25,26]**. Looking at PTN, the C_3-H_6 bond length of 1.10 Å corresponded closely with the standard C-H bond value, while the C_7-C_8 bond length of 1.52 Å showed normal single bond characteristics. The C_1=O_2 bond length of 1.204 Å also agreed well with the standard carbonyl bond length, confirming strong bond stability within the optimized structure. The slight deviations observed in some of the bond lengths may therefore be attributed to intramolecular charge transfer, steric effects, and redistribution of electron density within the studied adsorbates **[27]**.

3.1.1 Bond Properties of CNT and its Modified Surfaces

The modification of Carbon Nanotube (CNT) surfaces was done with the intent of tailoring its abilities to serve as a potential bio-sensor for better biomarker detection **[28]**. CNT was doped with copper (Cu) and nitrogen (N) individually and subsequently co-doped with both copper and nitrogen to form CuN@CNT. After modification, the bonds observed were visualized and the bond lengths recorded to compare the variations between CNT and its modified surfaces**. Table S2** focused on the bond distances of bare CNT and its modified forms (Cu@CNT, N@CNT, and CuN@CNT). The bare CNT exhibits typical sp^2 carbon character, with C-C bond distances around 1.45 Å and C=C bonds remaining around 1.40 Å. Upon nitrogen doping, N@CNT, the C-C bond decreased slightly to approximately 1.44 Å. After doping with copper (Cu@CNT), slight elongation of the C=C bond was observed which is explained by the interaction between the metal atom and the π-electron system of the CNT **[29]**. Copper introduced electron density into the system, disrupting the delocalized π-network and reducing the double bond character, thereby increasing bond distance **[30]**. Nitrogen doping (N@CNT) resulted in a slight shortening of the C-C bond, and nitrogen being more electronegative than carbon, electron density was withdrawn from adjacent atoms, resulting in a shorter and stronger C-C bond **[31]**. The co-doped system (CuN@CNT) exhibited a more pronounced structural distortion because of the combined electronic effects of both dopants (Cu and N). The presence of a relatively long C-Cu bond (~2.04 Å) compared to the standard length of 2.00 Å suggests a weak coordination interaction rather than a strong covalent bond **[32]**.

3.1.2 Bond Properties of Modified Surfaces Post Adsorption

Bond lengths of the surfaces post-adsorption were compared to those of CuN@CNT to assess significant changes in bond lengths after adsorption. **Table S3** presents the bond lengths of the CuN@CNT surface before and after interaction with the adsorbates. Prior to adsorption, the surface maintains relatively stable bond lengths consistent with a modified CNT structure. However, upon adsorption, noticeable changes occurred. The C-C and C=C bonds of the CNT framework exhibited slight elongation due to the nature of the interacting molecule. In CuN@CNT, C-C and C=C bond lengths were 1.45 Å and 1.36 Å respectively while C-C and C=C bond lengths post adsorption ranged from 1.45 Å to 1.46 Å and 1.36 Å to 1.37 Å respectively. These changes suggest electron redistribution within the system as charge may have been transferred between the adsorbate and the surfaces **[33]**. More important changes were observed in bonds involving the copper active site. Variations in the C-Cu bond length, such as a decrease from 2.04 Å to 2.03 Å in HXN or even more significant changes in LMN, suggest strengthening of the interaction due to adsorption. A shorter bond length generally indicates stronger binding, implying chemisorption, while smaller changes may point to weaker physisorption **[34]**. For the systems post-adsorption that C-N bonds were present in, compared to CuN@CNT there was a decrease in their lengths which was a result of increased electron density and stronger bonding due to electron withdrawal from neighboring atoms **[35]**. The values of C-N bonds across the interactions post-adsorption ranged from 1.40 Å to 1.52 Å, compared to CuN@CNT which had C-N bond length of 1.52 Å. Also, the formation of new bonds such as H-Cu, O-Cu, and C-Cu provides strong evidence of adsorption **[36]**. These interactions occur through lone pair donation (from oxygen or nitrogen atoms), π-electron interactions, or weak hydrogen coordination. In some cases, significant elongation of internal bonds within the adsorbate were observed, such as the increase in C=C bond length in the PTN system. The increase was as a result of a reduction in double bond character due to the interaction with the surface, often resulting from electron transfer into antibonding orbitals **[37]**. The absence of certain bonds (indicated by dashes) suggests structural rearrangement during adsorption **[38]**.

3.2 Reactivity Studies

3.2.1 HOMO-LUMO Studies

The electronic properties of CNT, its modified surfaces and CNT interactions were evaluated by examining their frontier molecular orbitals in order to predict its chemical reactivity, stability and interaction with other molecules **[39]**. HOMO-LUMO iso-surfaces were detected and visualized for CNT surfaces and interactions, represented in **Figure 1** and **Figure 2**. The energy gap (E_g) was calculated for CNT, its modified surfaces and surfaces post-adsorption. The values for the energy gap of these systems are presented in **Table 1**, which ranged from 2.44 eV to 3.08 eV where N@CNT had the lowest energy gap and MTN-CuN@CNT had the highest. CuN@CNT had an energy gap of 3.05 eV and being compared to the systems post-adsorption, there were slight changes but it still remained in normal range except for OTN-CuN@CNT. There was a significant decrease in the energy gap in OTN-CuN@CNT, this could be due to electron transfer between the dopants and the CNT which alters the distribution and energy of the frontier molecular orbitals **[40]**.

Quantum chemical methods were also carried out on the surfaces using **EQNs 2 – 5**. This study encompassed descriptors such as chemical potential (-μ), global hardness (η), global softness (σ), and electrophilicity (ω) which were used **[41]**. Global hardness of a system equals the stability of that system while global softness equals the reactivity. A compound or complex with great stability and low reactivity is said to be chemically hard while a compound or complex with low stability and great reactivity is said to be chemically soft **[42]**. Chemical potential is the measure of the tendency of a molecule to react or change phase, in other words the tendency for a system to use electrons or be involved in a chemical reaction **[43]**. Electrophilicity is the willingness of molecules or compounds to accept electrons. Global hardness and softness were also calculated to support the energy gap value of the systems, confirming the properties of the system. The global hardness across all systems ranged from 1.22 eV to 1.54 eV, while the global softness ranged from 0.32 eV^{-1} to 0.41 eV^{-1} giving insight to the stability and reactivity abilities of these systems, respectively. As observed in Table 1, the systems showcase more stability than reactivity. From the analysis it was observed that the systems post adsorption maintained a relatively low energy gaps when compared to CuN@CNT, with global hardness and global softness giving insight to the stability and reactivity of the systems. Values for these parameters were also relatively low

compared to the co-doped CuN@CNT. The lower energy gap is indicative of increased conductivity change upon adsorption, which is desirable for signal transduction in a sensor.

Table 1: Global Quantum chemical descriptors of CNT, its modified surfaces and interactions

Surfaces							
	E_{LUMO} (eV)	E_{HOMO} (eV)	E_g (eV)	-μ (eV)	η (eV)	σ (eV^{-1})	ω (eV)
CNT	-2.483	-5.538	3.05	-4.01	1.52	0.33	5.26
Cu@CNT	-2.899	-5.674	2.77	-4.28	1.38	0.36	6.62
N@CNT	-2.161	-4.603	2.44	-3.38	1.22	0.41	4.68
CuN@CNT	-2.272	-5.328	3.05	-3.80	1.53	0.33	4.72
Interactions							
	E_{LUMO} (eV)	E_{HOMO} (eV)	E_g (eV)	-μ (eV)	η (eV)	σ (eV)	ω (eV)
HXN-CuN@CNT	-2.271	-5.328	3.06	-3.80	1.53	0.33	4.72
LMN-CuN@CNT	-2.129	-5.185	3.05	-3.65	1.53	0.33	4.37
MTN-CuN@CNT	-2.224	-5.302	3.08	-3.76	1.54	0.32	4.60
OTN-CuN@CNT	-2.186	-5.155	2.97	-3.67	1.48	0.33	4.65
PTN-CuN@CNT	-2.165	-5.224	3.06	-3.69	1.53	0.32	4.46

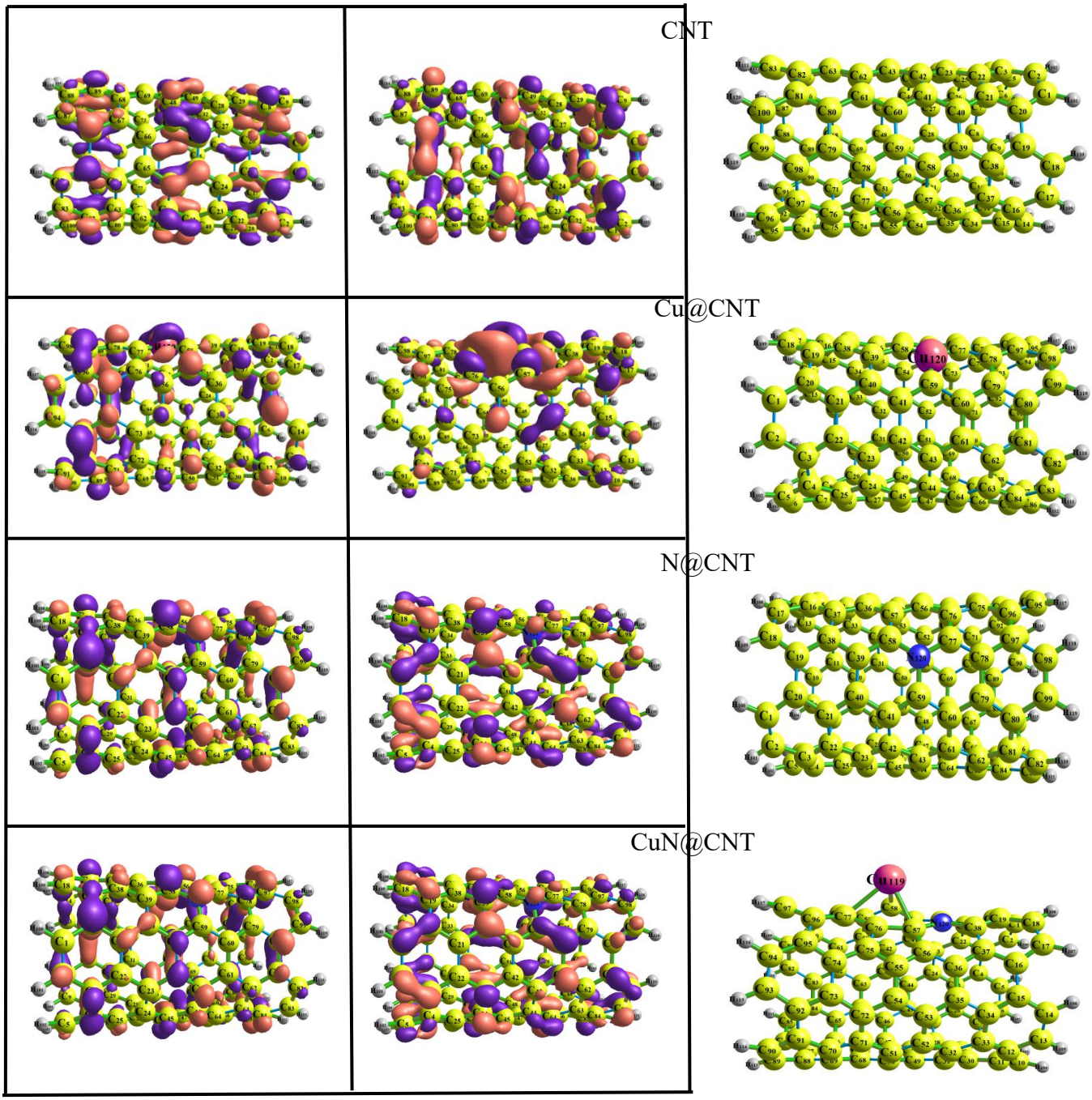


Figure 1: CNT and modified surfaces visualized, HOMO-LUMO iso-surface plots of CNT and its modified surfaces

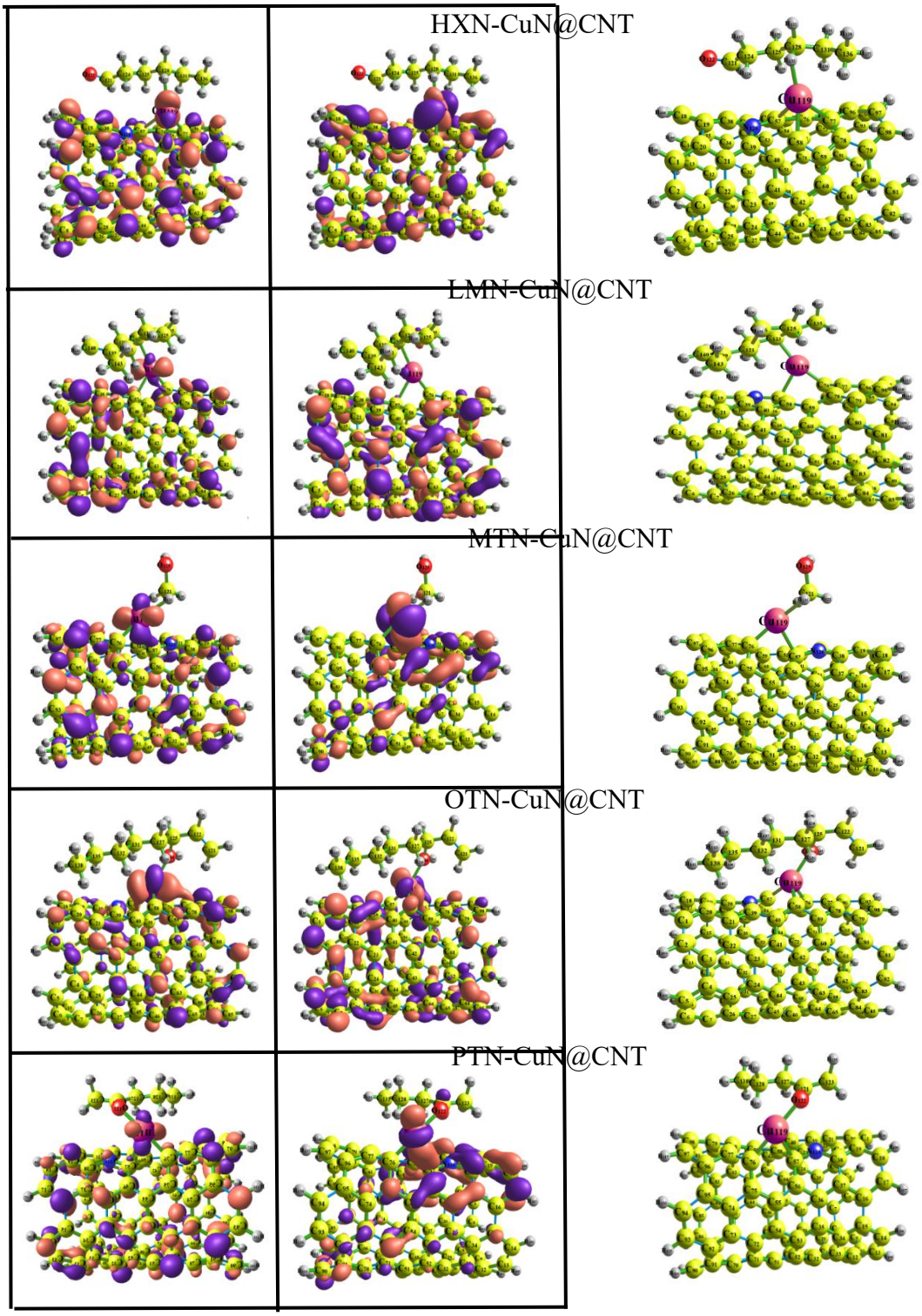


Figure 2: Surface post adsorption, HOMO-LUMO iso-surface plots of the CNT interactions

3.2.2 Natural Bond Orbital (NBO) Analysis

The electronic interactions formed between the studied liver cancer biomarkers and the surface of CuN@CNT were explained by performing the NBO analysis using the M06-2X/D3/Def2svp level of theory and the results presented in Table 2. The second order perturbation energy, E (^{2}), refers to the stabilization due to donor-acceptor electron delocalization, F(i,j) represents the strength of the orbital coupling **[44]**. The interactions observed give insights into electron donation from C-centered lone-pair and bonding orbitals into anti-bonding orbitals, illustrating the electronic redistribution at the biomarker-surface interface **[44,45]**. For HXN-CuN@CNT, the electron donation from the Cu-centered lone-pair (π) orbitals to the sigma antibonding ones gave E (^{2}) values between 0.25-0.36 kcal/mol. The values are indicative of weak non-covalent type interactions between LP (3) Cu_{119} and the sigma antibonding orbital of C_{58}-C_{59}, with E (^{2}) = 0.36 kcal/mol and F(i,j) = 0.017 a.u. This suggests that the Cu active site is directly involved in the electronic interaction with HXN **[46]**. The orbital delocalization of LMN-CuN@CNT was found to be stronger with E (^{2}) values of 0.58-0.73 kcal/mol. The most important contribution was the donation by C_{75}- C_{76} pi orbital to the C_{123}-C_{124} pi antibonding orbital with E ($^{2)}$ = 0.73 kcal/mol. Furthermore, the F(i,j) value for the interaction between the sigma bonding orbital of C_{76}-Cu_{119} and the sigma antibonding orbital of C_{122}-H_{134} was found to be equal to 0.027 a.u. The results suggest that there exist a pi-electron delocalization and a coupling of the Cu-associated orbital between LMN and CuN@CNT is present **[47]**. On the other hand, the orbital interaction was found to be comparatively weaker in the case of OTN-CuN@CNT, which exhibited E (^{2}) of 0.25-0.45 kcal/mol. The highest one was to the pi anti-bonding orbital of C_{56}–C_{57}, which was donated from LP (1) Cu_{119} with E (^{2}) = 0.45 kcal/mol and F(i,j) = 0.015 a.u. The lower E (^{2}) values compared to LMN, suggest less pronounced donor-acceptor delocalization and weaker orbital coupling between the OTN and CuN@CNT surface **[46]**. The strongest individual NBO interaction was observed for MTN-CuN@CNT with E (^{2}) of 1.72 kcal/mol and F(i,j) of 0.039 a.u. This is the maximum stabilization and orbital coupling in the system studied, and thus, it is a particularly strong electronic interaction between MTN and the CuN@CNT surface. For PTN-CuN@CNT, the Cu-mediated delocalization was also found to be quite significant with a donation of LP (4) Cu_{119} into the pi antibonding orbital of C_{57}-C_{58} equal to 1.11 kcal/mol **[48]**. The results show that the interactions between the biomarker and the surface are described by different orbital pathways,

with the Cu-centered lone-pair donation pathway being more relevant in the case of HXN, OTN and PTN, and pi-electron delocalization pathway more relevant in the case of LMN and MTN.

Table 2: NBO analysis highlighting charge transfer between bonding and antibonding orbitals (σ, π) of the adsorbent and adsorbate

Systems	**Donor(i)**	**Acceptor (j)**	**E (2) kcal/mol**	**E(j)-E(i) a.u**	**F(i,j) a.u**
HXN-CuN@CNT	LP(1)Cu_{119}	σ*C_{75} - C_{76}	0.25	0.96	0.014
	LP(2)Cu_{119}	σ*C_{58} – C_{59}	0.30	1.03	0.016
	LP(3)Cu_{119}	σ*C_{58} – C_{59}	0.36	1.02	0.017
LMN-CuN@CNT	σC_{57} -C_{58}	σ*C_{121} – H_{33}	0.58	1.23	0.026
	πC_{75} – C_{76}	π*C_{123} - C_{124}	0.73	0.42	0.017
	σC_{76} -Cu_{119}	σ*C_{122} – H_{134}	0.70	1.21	0.027
MTN-CuN@CNT	πC_{39} – C_{40}	σ*C_{121} – H_{122}	1.72	0.87	0.039
	σC_{56} -C_{57}	σ*C_{121} – O_{125}	0.62	1.17	0.024
	LP(1)Cu_{119}	σ*C_{121} – H_{124}	0.62	1.18	0.024
OTN-CuN@CNT	LP(1)Cu_{119}	π*C_{56} – C_{57}	0.45	0.46	0.015
	LP(2)Cu_{119}	π*C_{56} – C_{57}	0.28	0.43	0.012
	LP(2)Cu_{119}	σ*C_{75} – C_{76}	0.25	1.09	0.015
PTN-CuN@CNT	LP(2)Cu_{119}	σ*C_{75} – C_{76}	0.79	1.02	0.025
	LP(2)Cu_{119}	σ*C_{76} – C77	0.43	0.99	0.018
	LP(4)Cu_{119}	π*C_{57} – C_{58}	1.11	0.38	0.021

3.2.3 Molecular Electrostatic Potential (MESP) Analysis

MESP was carried out post adsorption to identify the electrophilic and the nucleophilic regions post adsorption using GaussView 6.0.16 and Gaussian 09W. The electron poor (electrophilic) regions are susceptible to nucleophilic attack, while the electron rich (nucleophilic) regions are susceptible to electrophilic attack **[49]**. These regions are represented by specific colors which have specific meanings to explain what goes on in the areas where they appear, and the colors that appear are usually blue, green and red. Blue representing the electrophilic region, is an electron poor region and also where nucleophiles attack. Green is an area of zero electrostatic potential, in other words the neutral region. Red is the represents the electron rich region which is the nucleophilic region where electrophiles attack **[50]**. As shown in **Figure 3** we can observe green and blue across all interactions where the green appears consistently in the middle of the CNT cage, indicating the area of zero electrostatic potential **[51]**. Blue indicating the electron poor region appears in-between the Cu_{119}, atom of the CNT cage and the hydrogen atoms in HXN of HXN-CuN@CNT. In LMN-CuN@CNT, blue surrounds the Cu_{119}, H_{129} and H_{133} atoms. In OTN-CuN@CNT and PTN-CuN@CNT, blue appears in the center in-between the Cu_{119} atom from the CNT cage and the carbon and hydrogen molecules of the adsorbate, but partially covers the O_{144}, H_{129} and H_{145} atoms of OXN-CuN@CNT and the Cu_{119} atom of PTN-CuN@CNT. Whereas in MTN-CuN@CNT, blue surrounds the Cu_{119} atom solely. These regions are electron poor and in need of electrons. Red which represents electron rich sites is not found, this could be due to the presence of copper which withdraws electron density from nearby atoms (oxygen or nitrogen) and acts as an electron acceptor **[52]**. The predominance of blue post-adsorption is an indication of the region where adsorption occurred. The electrostatic potential ranges for the compounds post adsorption were -1.848 to 1.848, -1.210 to 1.210, -1.822 to 1.822, -1.004 to 1.004 and -2.348 to 2.348 for HXN-CuN@CNT, LMN-CuN@CNT, MTN-CuN@CNT, OTN-CuN@CNT and PTN-CuN@CNT respectively, indicating zero electrostatic potential.

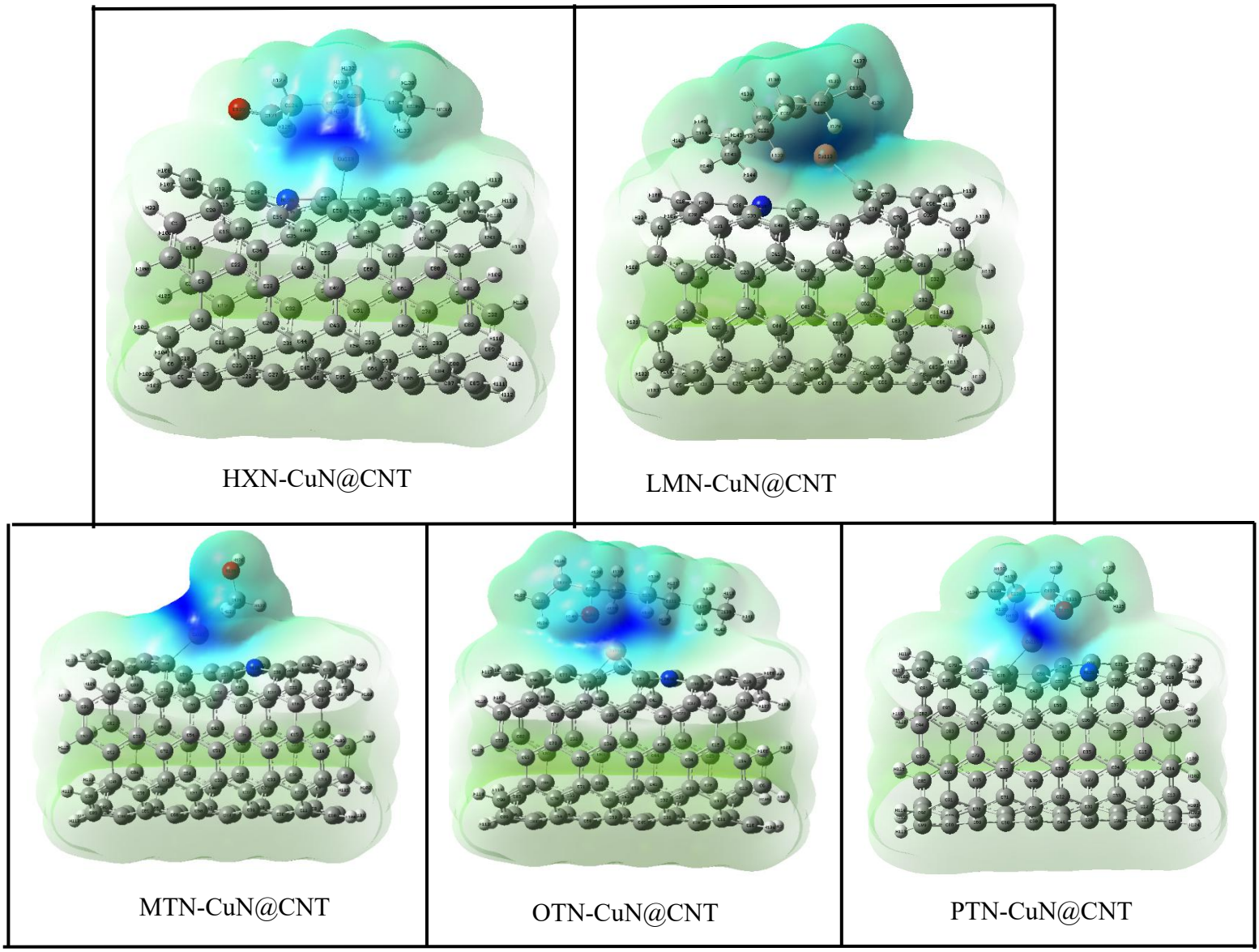


Figure 3: MESP plots of the surfaces post-adsorption

3.3 Non-Covalent Interaction (NCI) Analysis

NCI analysis was carried out post-adsorption to understand the relationship between the adsorbate and adsorbent. As represented in **Figure 4,** red, green and blue regions are observed. The red indicates strong repulsion/clash, blue indicates stronger attractive interactions often associated with hydrogen bonding and green is an indication of weak van der Waals **[53]**. In **Figure 4**, we see these colors present across all interactions., but some colors in more proportion than others. The presence of these 3 colors suggested that the adsorption was not governed by a single interaction type **[54]**. Weak van der Waals are predominant in HXN-CuN@CNT, LMN-CuN@CNT, OTN-CuN@CNT and PTN-CuN@CNT, while in MTN-CuN@CNT red is more predominant than the other colors. The van der Waals forces present contribute to the stability of the interactions, and with the presence of blue in-between the adsorbate and the adsorbent which indicates stronger attractive interactions. The NCI results are consistent with significant non-covalent stabilization supplementing weaker orbital level interactions **[55,56]**.

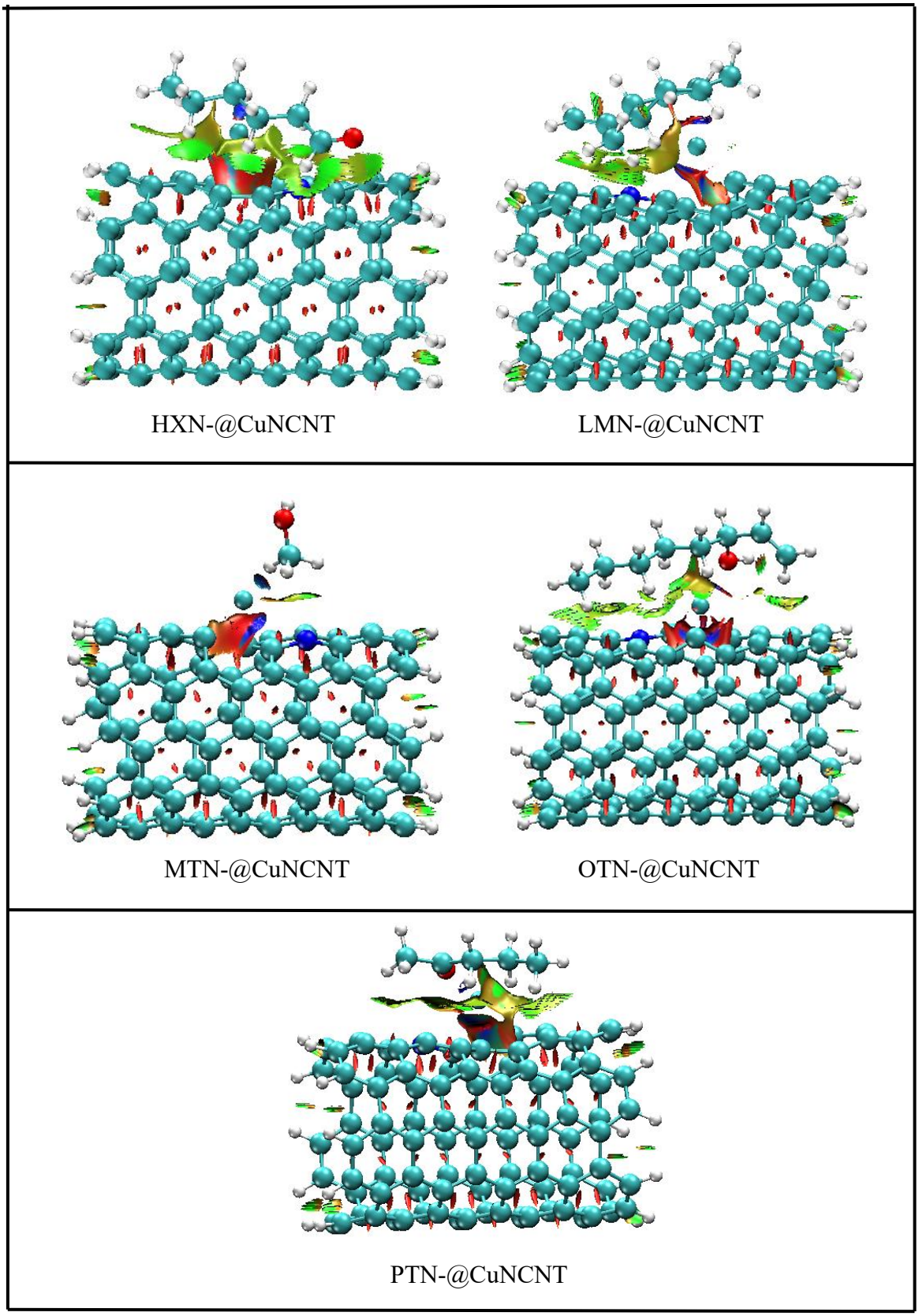


Figure 4: NCI analysis of the studied analysis using RDG gradient

3.4 Adsorption studies

As observed in **Table 3**, all systems post adsorption showcased negative adsorption energy values, confirming a thermodynamically favorable and exothermic interaction. Negative adsorption energy indicates favorable adsorption while positive adsorption energy indicates unfavorable adsorption, which implies the more negative the value the stronger the interaction and stability **[57]**. HXN-CuN@CNT, LMN-CuN@CNT, MTN-CuN@CNT, OTN-CuN@CNT, and PTN-CuN@CNT had adsorption energies of -1.10 eV, -2.85 eV, -2.50 eV, -0.85 eV and -2.78 eV respectively with LMN-CuN@CNT being the most negative, having a value of -2.85 eV. Adsorption energy less than -1.0 eV suggests chemisorption, which implies strong chemical interaction and stability while adsorption energy greater than -1.0 eV suggests physisorption, which implies weak interaction and stability **[58]**. Liu *et al.,* (2011) examined nitrogen doped SWCNTs on substrates, and results showed that nitrogen significantly changed the properties of the SWCNTs **[59]**. The study showed that nitrogen doped SWCNTs compared to pristine SWCNTs showcased enhanced sensitivity and selectivity for electrochemical detection of some electrophilic species including water and oxygen. Verma *et al.,* (2024) investigated the ability of transition metal and hetero atoms co-doped SWCNTs for hydrogen adsorption, where Au/Ag/Cu/B/N doped/co-doped SWCNTs systems were assessed. The study revealed that the modified systems possessed good hydrogen sensing abilities with Ag-NCNT having better hydrogen storage **[60]**. These findings are consistent with the fact that doped SWCNTs with nitrogen and copper have better sensing potentials over pristine SWCNTs. Li *et al.,* (2022) in their study on facile synthesis of copper and carbon co-doped peanut shell-like Mo_2C/Mo_3P electrocatalysts for ultra-sensitive ampere-metric detection of hydrogen peroxide reported that the good electrochemical sensing performance was mainly due to the synergism of the studied materials together with copper and carbon dual-doping **[61]**. This highlights the function of copper in enhancing the sensing abilities of peanut shell-like electrocatalyst in the detection of hydrogen peroxide.

These studies validate the usefulness of the modification of SWCNTs with nitrogen and or copper alongside single and dual doping involving copper, enhancing sensing performances of studied materials, therefore, increasing the potential for the studied compounds to be used as sensors.

Table 3: Adsorption energies of the studied CNT adsorbed surfaces

Interactions	**$E_{complex}$ (a.u)**	**$E_{surface}$ (a.u)**	**$E_{molecule}$ (a.u)**	**E_{ads} (a.u)**	**E_{ads} (eV)**
HXN-CuN@CNT	-5748.16	-5437.43	-310.68	-0.04	-1.10
LMN-CuN@CNT	-5827.72	-5437.43	-390.19	-0.10	-2.85
MTN-CuN@CNT	-5553.09	-5437.43	-115.57	-0.09	-2.50
OTN-CuN@CNT	-5826.66	-5437.43	-389.20	-0.03	-0.85
PTN-CuN@CNT	-5708.97	-5437.43	-271.44	-0.10	-2.78

3.5 Solvation analysis

Solvation study was carried out on the studied interactions using the conductor-like polarizable continuum model (CPCM) to determine their stability in a solution and thermodynamic favorability which in turn provides insight to their biosensing abilities outside gas phase **[62]**.

From the values presented in **Table** 4, all of the interactions show negative solvation energies, which means that their movement from gas phase into solution was favorable based on Gibbs Free Energy **[63]**. From **Table 4** HXN-CuN@CNT, LMN-CuN@CNT, MTN-CuN@CNT, OTN-CuN@CNT, and PTN-CuN@CNT had solvation energies of -0.75 eV, -0.65 eV, -0.78 eV, -0.69 eV and -0.66 eV respectively. The results from the solvation energies were negative, indicating thermodynamic stability of the doped systems in solution, supporting their potential compatibility with biological (aqueous) environment **[62,64]**. When comparing them, MTN-CuN@CNT was the most negative, with a value of -0.78 eV, followed by HXN-CuN@CNT. These negative values are an indication of their stability in solvents, therefore, their potential ability to move in biological targets.

Table 4: Solvation energies of the studied CNT adsorbed surfaces

Interactions	**E_{water} (a.u)**	**E_{gas} (a.u)**	**E_{sol} (a.u)**	**E_{sol} (eV)**
HXN-CuN@CNT	-5748.19	-5748.16	-0.027	-0.75
LMN-CuN@CNT	-5827.75	-5827.72	-0.023	-0.65
MTN-CuN@CNT	-5553.09	-5553.06	-0.028	-0.78
OTN-CuN@CNT	-5826.69	-5826.66	-0.025	-0.69
PTN-CuN@CNT	-5708.99	-5708.97	-0.024	-0.66

4.0 Conclusion

This study investigated the structural, electronic, and adsorption properties of Cu- and N-co-doped carbon nanotubes (CuN@CNT) as a candidate biosensing material for liver cancer biomarkers, using DFT methods. Geometry optimization showed that bond distances across the studied complexes remained within standard ranges, indicating structurally stable adducts. Adsorption energy calculations yielded negative values for all five biomarker systems, confirming thermodynamically favorable, exothermic adsorption onto the CuN@CNT surface, with MTN, LMN, and PTN showing the most favorable binding. NBO analysis further identified Cu-centered lone-pair donation and π-electron delocalization as the dominant orbital interaction pathways, with MTN exhibiting the strongest individual donor-acceptor stabilization (E(2) = 1.72 kcal/mol) among the biomarkers studied, followed by PTN, LMN, OTN, and HXN. MESP mapping indicated electron-poor regions concentrated near the Cu active site and adjacent carbon atoms post-adsorption, while NCI analysis revealed a combination of van der Waals, steric, and weak attractive interactions across all systems, indicating that adsorption is governed by multiple non-covalent interaction types rather than a single dominant mechanism. Solvation studies showed negative solvation free energies for all complexes, supporting their thermodynamic stability in an

aqueous environment relevant to physiological conditions. Taken together, these results suggest that CuN@CNT forms stable, energetically favorable, and electronically active interactions with the studied liver cancer biomarkers, supporting its potential as a biosensing platform. Further experimental validation, along with kinetic and selectivity studies, is recommended to confirm the practical biosensing performance of CuN@CNT suggested by these computational findings

Conflict Of Interest

The authors declare that there is no conflict of interest or financial interest regarding the publication of this manuscript

Funding

This research paper has not received any kind of funding.

Declaration

Ethics, consent to participate and consent to publish declarations: not applicabble

References

1. Sriharikrishnaa, S., Suresh, P. S., & Prasada K, S. (2023). An introduction to fundamentals of cancer biology. In *Optical Polarimetric modalities for biomedical research* (pp. 307-330). Cham: Springer International Publishing. https://doi.org/10.1007/978-3-031-31852-8_11
2. Hassanpour, S. H., & Dehghani, M. (2017). Review of cancer from perspective of molecular. *Journal of cancer research and practice*, *4*(4), 127-129. https://doi.org/10.1016/j.jcrpr.2017.07.001
3. Saini, A., Kumar, M., Bhatt, S., Saini, V., & Malik, A. (2020). Cancer causes and treatments. *Int J Pharm Sci Res*, *11*(7), 3121-3134. 10.13040/IJPSR.0975-8232.11(7).3121-34
4. Rajput, J. M. (2023). Cancer: a comprehensive review. *International Journal of Research in Pharmacy and Allied Science*, *1*(3), 42-49.
5. Li, Y., Liu, F., Cai, Q., Deng, L., Ouyang, Q., Zhang, X. H. F., & Zheng, J. (2025). Invasion and metastasis in cancer: molecular insights and therapeutic targets. *Signal transduction and targeted therapy*, *10*(1), 57. https://doi.org/10.1038/s41392-025-02148-4
6. Chandraprasad, M. S., Dey, A., & Swamy, M. K. (2022). Introduction to cancer and treatment approaches. In *Paclitaxel* (pp. 1-27). Academic Press. 10.1016/B978-0-323-90951-8.00010-2
7. Rahman, M. S., Suresh, S., & Waly, M. I. (2018). Risk factors for cancer: Genetic and environment. In *Bioactive components, diet and medical treatment in cancer prevention* (pp. 1-23). Cham: Springer International Publishing. https://doi.org/10.1007/978-3-319-75693-6_1
8. Koo, M. M., Hamilton, W., Walter, F. M., Rubin, G. P., & Lyratzopoulos, G. (2018). Symptom signatures and diagnostic timeliness in cancer patients: a review of current evidence. *Neoplasia*, *20*(2), 165-174. https://doi.org/10.1016/j.neo.2017.11.005
9. Liyanage, T., Qamar, A. Z., & Slaughter, G. (2020). Application of nanomaterials for chemical and biological sensors: A review. *IEEE Sensors Journal*, *21*(11), 12407-12425. 10.1109/JSEN.2020.3032952.

10. Gupta, N., Gupta, S. M., & Sharma, S. K. (2019). Carbon nanotubes: synthesis, properties and engineering applications. *Carbon Letters*, *29*(5), 419-447. https://doi.org/10.1007/s42823-019-00068-2
11. Kharlamova, M. V., & Eder, D. (2020). Carbon nanotubes: synthesis, properties, and new developments in research. *Synthesis and Applications of Nanocarbons*, 107-147. **https://doi.org/10.1002/9781119429418.ch4**
12. Bati, A. S., Yu, L., Batmunkh, M., & Shapter, J. G. (2018). Synthesis, purification, properties and characterization of sorted single-walled carbon nanotubes. *Nanoscale*, *10*(47), 22087-22139. https://doi.org/10.1039/c8nr07379a
13. Tang, D. M., Cretu, O., Ishihara, S., Zheng, Y., Otsuka, K., Xiang, R., ... & Golberg, D. (2024). Chirality engineering for carbon nanotube electronics. *Nature Reviews Electrical Engineering*, *1*(3), 149-162. https://doi.org/10.1038/s44287-023-00011-8
14. Norizan, M. N., Moklis, M. H., Ngah Demon, S. Z., Halim, N. A., Samsuri, A., Mohamad, I. S., ... & Abdullah, N. (2020). Carbon nanotubes: Functionalisation and their application in chemical sensors. *RSC advances*, *10*(71), 43704-43732. https://doi.org/10.1039/d0ra09438b
15. Aasi, A., Aasi, E., Aghaei, S. M., & Panchapakesan, B. (2022). CNT biodevices for early liver cancer diagnosis based on biomarkers detection-a promising platform. *Journal of Molecular Graphics and Modelling*, *114*, 108208 https://doi.org/10.1016/j.jmgm.2022.108208
16. Rahimi, R., & Solimannejad, M. (2025). B3C2N3 monolayer as a potential biosensor for the sensitive and selective detection of liver cancer biomarkers: A DFT study. *Materials Science in Semiconductor Processing*, *186*, 109025. https://doi.org/10.1016/j.mssp.2024.109025
17. Alghoul, I., Hussain, T., Nazir, S., & Tit, N. (2025). Efficient detection of gastric cancer biomarkers on functionalized carbon nanoribbons using DFT analysis. *Scientific reports*, *15*(1), 13173. https://doi.org/10.1038/s41598-025-97518-x
18. Fu, L., Ju, Z., Yu, M., Luo, H., Zhang, C., Zhang, X., ... & Ge, C. (2022). Cellulose regeneration in imidazolium-based ionic liquids and antisolvent mixtures: A density functional theory study. *ACS omega*, *7*(46), 42170. 10.1021/acsomega.2c04915

19. Dennington, R. D. I. I., Keith, T. A., & Millam, J. M. (2016). GaussView 6.0. 16. *Semichem Inc.: Shawnee Mission, KS, USA*, 143-150.
20. Chemcraft - graphical software for visualization of quantum chemistry computations. Version 1.8, build 682. https://www.chemcraftprog.com
21. Gaussian 09, Revision A.02, M. J. Frisch, G. W. Trucks, H. B. Schlegel, G. E. Scuseria, M. A. Robb, J. R. Cheeseman, G. Scalmani, V. Barone, G. A. Petersson, H. Nakatsuji, X. Li, M. Caricato, A. Marenich, J. Bloino, B. G. Janesko, R. Gomperts, B. Mennucci, H. P. Hratchian, J. V. Ortiz, A. F. Izmaylov, J. L. Sonnenberg, D. Williams-Young, F. Ding, F. Lipparini, F. Egidi, J. Goings, B. Peng, A. Petrone, T. Henderson, D. Ranasinghe, V. G. Zakrzewski, J. Gao, N. Rega, G. Zheng, W. Liang, M. Hada, M. Ehara, K. Toyota, R. Fukuda, J. Hasegawa, M. Ishida, T. Nakajima, Y. Honda, O. Kitao, H. Nakai, T. Vreven, K. Throssell, J. A. Montgomery, Jr., J. E. Peralta, F. Ogliaro, M. Bearpark, J. J. Heyd, E. Brothers, K. N. Kudin, V. N. Staroverov, T. Keith, R. Kobayashi, J. Normand, K. Raghavachari, A. Rendell, J. C. Burant, S. S. Iyengar, J. Tomasi, M. Cossi, J. M. Millam, M. Klene, C. Adamo, R. Cammi, J. W. Ochterski, R. L. Martin, K. Morokuma, O. Farkas, J. B. Foresman, and D. J. Fox, Gaussian, Inc., Wallingford CT, 2016.
22. Tian Lu, Feiwu Chen, Multiwfn: A Multifunctional Wavefunction Analyzer, J. Comput. Chem. 33, 580-592 (2012) 10.1002/jcc.22885
23. Varadwaj, P. R., Varadwaj, A., & Jin, B. Y. (2014). Significant evidence of C⋯ O and C⋯ C long-range contacts in several heterodimeric complexes of CO with CH 3–X, should one refer to them as carbon and dicarbon bonds!. *Physical Chemistry Chemical Physics*, *16*(32), 17238-17252. https://doi.org/10.1039/c4cp01775g
24. Schwarz, H. (2017). Metal-mediated activation of carbon dioxide in the gas phase: Mechanistic insight derived from a combined experimental/computational approach. *Coordination Chemistry Reviews*, *334*, 112-123. https://doi.org/10.1016/j.ccr.2016.03.009
25. Christensen, A. S., Kromann, J. C., Jensen, J. H., & Cui, Q. (2017). Intermolecular interactions in the condensed phase: Evaluation of semi-empirical quantum mechanical methods. *The Journal of Chemical Physics*, *147*(16). https://doi.org/10.1063/1.4985605

26. Alvarez, J. A. S., & Calaminici, P. (2025). A Review of Global Optimization Methods for Molecular Structures: Algorithms, Applications and Perspectives. *Journal of Computational Chemistry*, *46*(28), e70243. https://doi.org/10.1002/jcc.70243
27. Jagau, T. C. (2022). Theory of electronic resonances: fundamental aspects and recent advances. *Chemical Communications*, *58*(34), 5205-5224. https://doi.org/10.1039/d1cc07090h
28. Solangi, N. H., Karri, R. R., Mubarak, N. M., Mazari, S. A., & Sharma, B. P. (2024). Holistic insights into carbon nanotubes and MXenes as a promising route to bio-sensing applications. *Nanoscale*, *16*(46), 21216-21263. https://doi.org/10.1039/d4nr03008g
29. Li, C., Ji, Y., Wang, Y., Liu, C., Chen, Z., Tang, J., ... & Xia, C. (2023). Applications of metal–organic frameworks and their derivatives in electrochemical CO2 reduction. *Nano-Micro Letters*, *15*(1), 113. https://doi.org/10.1007/s40820-023-01092-8
30. Jiang, H., Shen, J., Sun, L., Li, J., Wang, W., Wang, L., & Liu, Q. (2025). Advances in molecular interfacial engineering of heterojunctions for photocatalytic CO 2 reduction. *Green Chemistry*, *27*(24), 6989-7008. https://doi.org/10.1039/d5gc01228g
31. Varadwaj, P. R., Varadwaj, A., Marques, H. M., & Yamashita, K. (2022). The Nitrogen Bond, or the Nitrogen-Centered Pnictogen Bond: The Covalently Bound Nitrogen Atom in Molecular Entities and Crystals as a Pnictogen Bond Donor. *Compounds*, *2*(1), 80-110. https://doi.org/10.3390/compounds2010007
32. Asundi, A. S., Noonikara-Poyil, A., Phan, V. Q. H., Dias, H. R., & Sarangi, R. (2023). Understanding Copper (I)–Ethylene Bonding Using Cu K-Edge X-ray Absorption Spectroscopy. *Inorganic Chemistry*, *62*(47), 19298-19311. https://doi.org/10.1021/acs.inorgchem.3c02904
33. Sun, S., Zhang, Y., Shi, X., Sun, W., Felser, C., Li, W., & Li, G. (2024). From charge to spin: an in-depth exploration of electron transfer in energy electrocatalysis. *Advanced Materials*, *36*(37), 2312524. https://doi.org/10.1002/adma.202312524
34. Liu, S., Liu, J., Liu, X., Shang, J. X., Yu, R., & Shui, J. (2022). Non-classical hydrogen storage mechanisms other than chemisorption and physisorption. *Applied Physics Reviews*, *9*(2). https://doi.org/10.1063/5.0088529
35. Xu, Y., Ma, Y., Chen, X., Wu, K., Wang, K., Shen, Y., ... & Zhang, Y. (2024). Regulating reactive oxygen intermediates of Fe− N− C SAzyme via second-shell coordination for

selective aerobic oxidation reactions. *Angewandte Chemie*, *136*(36), e202408935. https://doi.org/10.1002/ange.202408935

36. Dai, Z., Lai, K., Li, X., Ge, L., Li, L., Liu, Z., & Li, N. (2026). Asymmetric adsorption site and cu vacancy regulation in La–cu Nanospheres to promote CO2 Electroreduction performance with ultrahigh CH4 selectivity. *Advanced Functional Materials*, *36*(5), e14227. https://doi.org/10.1002/adfm.202514227
37. Sun, S., Zhang, Y., Shi, X., Sun, W., Felser, C., Li, W., & Li, G. (2024). From charge to spin: an in-depth exploration of electron transfer in energy electrocatalysis. *Advanced Materials*, *36*(37), 2312524. https://doi.org/10.1002/adma.202312524
38. Cheng, Z., Hu, Z., & Jiao, N. (2025). Molecular ring remodeling through C–C bond cleavage. *Accounts of Chemical Research*, *58*(6), 1003-1022. https://doi.org/10.1021/acs.accounts.4c00846
39. Chen, Y., Han, J., & Yang, X. (2023). DFT simulation of structure stability and nitrogen oxide adsorption for nitrogen and oxygen co-modified carbon nanotubes. *Surfaces and Interfaces*, *42*, 103498. https://doi.org/10.1016/j.surfin.2023.103498
40. Zhang, A., Wu, J., Xue, L., Yan, S., & Zeng, S. (2020). Probing heteroatomic dopant-activity synergy over Co3O4/doped carbon nanotube electrocatalysts for oxygen reduction reaction. *Inorganic Chemistry*, *59*(1), 403-414. https://doi.org/10.1021/acs.inorgchem.9b02663
41. Nadr, R. B., Abdulrahman, B. S., Azeez, Y. H., Omer, R. A., & Kareem, R. O. (2024). Quantum chemical calculation for synthesis some thiazolidin-4-one derivatives. *Journal of Molecular Structure*, *1308*, 138055. https://doi.org/10.1016/j.molstruc.2024.138055
42. Aziz, K. N., Ahmed, K. M., Omer, R. A., Qader, A. F., & Abdulkareem, E. I. (2025). A review of coordination compounds: structure, stability, and biological significance. *Reviews in Inorganic Chemistry*, *45*(1), 1-19. https://doi.org/10.1515/revic-2024-0035
43. Baerends, E. J. (2022). Chemical potential, derivative discontinuity, fractional electrons, jump of the Kohn–Sham potential, atoms as thermodynamic open systems, and other (mis) conceptions of the density functional theory of electrons in molecules. *Physical Chemistry Chemical Physics*, *24*(21), 12745-12766. https://doi.org/10.1039/d2cp01585d

44. Reed, A. E., Curtiss, L. A., & Weinhold, F. (1988). Intermolecular interactions from a natural bond orbital, donor-acceptor viewpoint. *Chemical reviews*, *88*(6), 899-926. https://doi.org/10.1021/cr00088a005
45. Rahimi, R., & Solimannejad, M. (2025). B3C2N3 monolayer as a potential biosensor for the sensitive and selective detection of liver cancer biomarkers: A DFT study. *Materials Science in Semiconductor Processing*, *186*, 109025. https://doi.org/10.1016/j.mssp.2024.109025
46. Aasi, A., Aasi, E., Aghaei, S. M., & Panchapakesan, B. (2022). CNT biodevices for early liver cancer diagnosis based on biomarkers detection – a promising platform. *Journal of Molecular Graphics and Modelling*, 114, 108208. (identifies hexanal as a liver cancer breath biomarker studied via DFT on CNT surfaces) https://doi.org/10.1016/j.jmgm.2022.108208
47. O'Hara, M. E., Del Río, R. F., Holt, A., Pemberton, P., Shah, T., Whitehouse, T., & Mayhew, C. A. (2016). Limonene in exhaled breath is elevated in hepatic encephalopathy. *Journal of breath research*, *10*(4), 046010. https://doi.org/10.1088/1752-7155/10/4/046010
48. Stavropoulos, G., van Munster, K., Ferrandino, G., Sauca, M., Ponsioen, C., van Schooten, F. J., & Smolinska, A. (2021). Liver impairment—the potential application of volatile organic compounds in hepatology. *Metabolites*, *11*(9), 618. https://doi.org/10.3390/metabo11090618
49. Frost, S. J., Yik, B. J., Dood, A. J., de Arellano, D. C. R., Fields, K. B., & Raker, J. R. (2023). Evaluating electrophile and nucleophile understanding: a large-scale study of learners' explanations of reaction mechanisms. *Chemistry Education Research and Practice*, *24*(2), 706-722. https://doi.org/10.1039/d2rp00327a
50. Suresh, C. H., Remya, G. S., & Anjalikrishna, P. K. (2022). Molecular electrostatic potential analysis: A powerful tool to interpret and predict chemical reactivity. *Wiley Interdisciplinary Reviews: Computational Molecular Science*, *12*(5), e1601. https://doi.org/10.1002/wcms.1601
51. Gwyther, R. E., Côté, S., Lee, C. S., Miao, H., Ramakrishnan, K., Palma, M., & Dafydd Jones, D. (2024). Optimising CNT-FET biosensor design through modelling of

biomolecular electrostatic gating and its application to β-lactamase detection. *Nature Communications*, *15*(1), 7482. https://doi.org/10.1038/s41467-024-51325-6

52. Xie, Z. L., Gupta, N., Niklas, J., Poluektov, O. G., Lynch, V. M., Glusac, K. D., & Mulfort, K. L. (2023). Photochemical charge accumulation in a heteroleptic copper (i)-anthraquinone molecular dyad via proton-coupled electron transfer. *Chemical Science*, *14*(37), 10219-10235. https://doi.org/10.1039/d3sc03428c
53. Johnson, E. R., Keinan, S., Mori-Sánchez, P., Contreras-García, J., Cohen, A. J., & Yang, W. (2010). Revealing non-covalent interactions. *Journal of the American Chemical Society*, *132*(18), 6498. 10.1021/ja100936w
54. Al-Otaibi, J. S., Mary, Y. S., Mary, Y. S., Mondal, A., Acharjee, N., & Balachandar, S. (2022). Investigation of the adsorption of a DNA based purine derivative on N/B-doped coronene and coronene by means of DFT and NCI interaction analysis. *Journal of Molecular Liquids*, *367*, 120373. 10.1016/j.molliq.2022.120373
55. Hermann, J., DiStasio Jr, R. A., & Tkatchenko, A. (2017). First-principles models for van der Waals interactions in molecules and materials: Concepts, theory, and applications. *Chemical Reviews*, *117*(6), 4714-4758. https://doi.org/10.1021/acs.chemrev.6b00446
56. Fu, C. (2026). Targeting colorectal cancer biomarkers in breath: DFT optimization of metal oxide nanoclusters for ultrasensitive sensing. *Journal of Nanoparticle Research*, *28*(7), 194. https://doi.org/10.1007/s11051-026-06708-9
57. Zhang, J., Yang, H. B., Zhou, D., & Liu, B. (2022). Adsorption energy in oxygen electrocatalysis. *Chemical Reviews*, *122*(23), 17028-17072. https://doi.org/10.1021/acs.chemrev.1c01003
58. Lv, W., Zhang, R., Sun, F., Guo, Y., Jiao, W., Wang, H., ... & Lv, B. (2025). Application of Physical Adsorption and Chemisorption Techniques in Heterogeneous Catalytic Research: A Review. *Kinetics and Catalysis*, *66*(2), 129-154. https://doi.org/10.1134/S0023158424602596
59. Liu, Y., Jin, Z., Wang, J., Cui, R., Sun, H., Peng, F., ... & Li, Y. (2011). Nitrogen-doped single-walled carbon nanotubes grown on substrates: evidence for framework doping and their enhanced properties. *Advanced Functional Materials*, *21*(5), 986-992. https://doi.org/10.1002/adfm.201002086

60. Verma, R., & Jaggi, N. (2024). Ability of transition metal and hetero atoms co-doped SWCNTs for hydrogen adsorption: A DFT study. *Journal of Physics and Chemistry of Solids*, *194*, 112244. https://doi.org/10.1016/j.jpcs.2024.112244
61. Li, B., Kong, D. R., Liu, L. H., Yang, M., Zhang, X. F., Deng, Z. P., ... & Gao, S. (2022). Facile synthesis of copper and carbon co-doped peanut shell-like Mo2C/Mo3P electrocatalysts for ultra-sensitive amperometric detection of hydrogen peroxide. *Microchemical Journal*, *181*, 107795. https://doi.org/10.1016/j.microc.2022.107795
62. Anzenbacher Jr, P., Prakash, A., George, S. M., Sartori, A. R., Zamkov, M., & Tarnovsky, A. N. (2025). Overcoming the Hydration and Solvation Problem in Ion Recognition and Binding: The Biomimetic Approach. *Accounts of Chemical Research*, *58*(17), 2792-2803. https://doi.org/10.1021/acs.accounts.5c00472
63. Lin, C., He, X., Xi, C., Zhang, Q., & Wang, L. W. (2024). Ion solvation free energy calculations based on first-principles molecular dynamics thermodynamic integration. *The Journal of Chemical Physics*, *160*(18). https://doi.org/10.1063/5.0191068
64. Pathania, V., Sharma, S., Vermani, B. K., Kaur, H., & Thakur, R. C. (2023). Investigating the solvation behavior of some perchlorates in non-aqueous medium and predicting their ion-solvation thermodynamics using Born formula. *Journal of Molecular Liquids*, *371*, 121067. https://doi.org/10.1016/j.molliq.2022.121067

Supplementary Files

This is a list of supplementary files associated with this preprint. Click to download.

- Supportinginfobiomarker.docx